INACTIVE SPACE OBJECT SHAPE ESTIMATION VIA ASTROMETRIC AND PHOTOMETRIC DATA FUSION

Richard Linares*
University at Buffalo, State University of New York, Amherst, NY, 14260-4400
Moriba K. Jah†
Air Force Research Laboratory, Kirtland AFB, New Mexico, 87117
John L. Crassidis‡
University at Buffalo, State University of New York, Amherst, NY, 14260-4400

This paper presents a method to determine the shape of a space object in orbit while simultaneously recovering the observed space object's inertial orientation and trajectory. This work studies a shape estimation approach based on octant triangulation applied to light curve and angles data fusion. The filter employs the Unscented estimation approach, reducing passively-collected electro-optical data to infer the unknown state vector comprised of the space object inertial-to-body orientation, position and their respective temporal rates. Recovering these characteristics and trajectories with sufficient accuracy is shown in this paper. The performance of this strategy is demonstrated via simulated scenarios.

MOTIVATION

In recent years space situational awareness, which is concerned with collecting and maintaining knowledge of all objects orbiting the Earth, has gained much attention. The U.S. Air Force collects the necessary data for space object catalog development and maintenance through a global network of radars and optical sensors. Due to the fact that a limited number of sensors are available to track a large number of space objects (SOs), the sparse data collected must be exploited to the fullest extent. Various sensors, such as radars, exist for SO state estimation, which typically includes position, velocity, and a non-conservative force parameter, B^*, analogous to a ballistic coefficient. Another piece of useful information is the estimation of the shape of an object, which requires knowledge of the attitude of the SO.

Shape estimation is an important issue in the observation of SOs, because the shape influences the dynamics of the object and may enables unique space object identification, beyond just using the object's translational states. There exists a number of methods for estimating the shape of an object. These methods vary in the sensor type used, technique used to resolve shape, and effective ranges for proper shape resolution. Radar-based methods have been extensively used for shape

*Graduate Student, Department of Mechanical & Aerospace Engineering. Email: linares2@buffalo.edu, Student Member AAS, Student Member AAS, Student Member AIAA.
†Senior Research Aerospace Engineer. Member AAS, Associate Fellow AIAA.
‡Professor, Department of Mechanical & Aerospace Engineering. Email: johnc@buffalo.edu, Member AAS, Associate Fellow AIAA.

estimation, which include radar cross-sectioning approaches[1] and range Doppler interferometry.[2] These techniques were first developed in the field of planetary radar astronomy to estimate the shape of natural satellites,[3] but were later applied to the imaging of artificial Earth orbiting satellites. These methods are limited to SOs that are larger than the radar's wavelength. SOs can be imaged in low-Earth orbits that are much larger in dimension than the wavelength of the radar signal. To image SOs smaller and farther than these ranges requires very powerful radar devices, making these economically unattractive.

Laser radar-based (LADAR) methods have also been used to estimate the shape of SOs. LADAR provides a three-dimensional scan of the object, which can resolve shape geometry at ranges of 1 km, returning a cloud of points of the measured relative position of an object. Reference [4] uses LADAR scans to perform a least squares fit of the LADAR returns to previously assembled point cloud models to estimate the shape of an SO. Reference [5] develops a filter approach to simultaneously estimate dynamic states, geometric shape, and mass model parameters of a satellite using multiple observations with LADAR sensors. In Ref. [5] a probabilistic map of the SO is constructed using a sensor uncertainty model and the dynamics experienced by the SO to estimate its shape. Using well modeled dynamical relationships of the SO provides enhancements to be implemented within a filter architecture in this shape estimation approach.[5]

Resolved images have been used to estimate the size and shape of satellites as well.[6] These methods work either directly with the pixels of the images or are used to identify features of the SO. Features, such as corners, edges and markers, are located and tracked temporally to estimate higher level motion and the structure of the rigid body.[7] The feature-based methods rely on continuously identifying and tracking higher level traits of the SO by using a Kalman filter to estimate feature location and motion parameters. Although these methods estimate the motion of features they do not by themselves provide a detailed estimate of the shape of the object and only give a sparse set of feature points of the object. Pixel-based methods rely on pixel-level information, and use the shading, texture and optical flow of the images to estimate the shape of an object at each time step using a monocular camera. Since these methods rely on pixel-level computations they typically involve very high-dimensional states and therefore are very computationally expensive. These methods are also very sensitive to pixel-level detail and are easily corrupted by unpredictable light intensities, reflective material and wrinkled surfaces. They require high resolution of the object to resolve meaningful shape estimates, and therefore are only effective for space-based sensors and or high resolution ground-based telescopes.

Light curves (the SO temporal brightness) have also been used to estimate the shape for an object. Light curve approaches have been studied to estimate the shape and state of asteroids.[8,9] Reference [10] uses light curves and thermal emissions to recover the three-dimensional shape of an object assuming its orientation with respect to the observer is known. The benefits of using a light curve-based approach over the aforementioned others is that it is not limited to larger objects in lower orbits and it can be applied to small and dim objects in higher orbits, such as geosynchronous. Here light curve data is considered for shape estimation, which is useful because it provides a mechanism to estimate both position and attitude, as well as their respective rates.[11,12]

There are several aspects of using light curve data (temporal photometry) that make it particularly advantageous for object detection, identification and tracking. Light curve data are the time-varying sensor wavelength-dependent apparent magnitude of energy (i.e. photons) scattered (reflected) off of an object along the line-of-sight to an observer. Because the apparent magnitude of the SO is a function of its size, orientation, and surface material properties, one or more of these characteristics

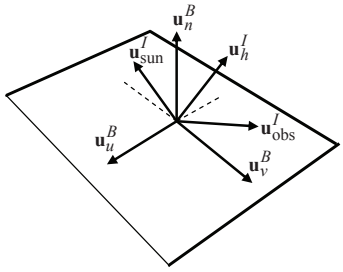

Figure 1. Reflection Geometry

should be recoverable from the photometric data. This can aid in the detection and identification of an SO after a catalog of spacecraft data with material properties is developed, and may also prove to be powerful for never-seen-before objects.

This work studies a shape estimation approach based on octant triangulation applied to light curve and angles data fusion. The translation, rotation, and shape parameters states of a SO are estimated using a UKF approach. The organization of this paper is as follows: first the shape model using a octant triangulation will be discussed, then system dynamical models are outlined, following this measurement models are shown including a CCD noise model, next the UKF used for this work is reviewed, and finally a simulation example is given.

SHAPE MODEL DEFINITION

The shape model considered in this work consists of a finite number a flat facets, where each facet has a set of basis vectors associated with it. These basis vectors are defined in Figure 1 and consist of three unit vectors $\mathbf{u}_n^B$, $\mathbf{u}_u^B$, and $\mathbf{u}_v^B$. The unit vector $\mathbf{u}_n^B$ points in the direction of the outward normal to the facet. For convex surfaces this model become more accurate as the number of facets are increased. The vectors $\mathbf{u}_u^B$ and $\mathbf{u}_v^B$ are in the plane of the facet. The space objects (SOs) are assumed to be rigid bodies and therefore the unit vectors $\mathbf{u}_n^B$, $\mathbf{u}_u^B$ and $\mathbf{u}_v^B$ do not change since they are expressed in the body frame.

The light curve and the solar radiation pressure (solar radiation pressure (SRP)) models discussed in the next sections require that these vectors be expressed in inertial coordinates and since the SO body is rotating, these vectors will change with respect to the inertial frame. The body vectors can be rotated to the inertial frame by the standard attitude mapping given by:

$$\mathbf{u}_i^B = A(\mathbf{q}_I^B)\mathbf{u}_k^I, \quad k = u,\, v,\, n \tag{1}$$

where $A(\mathbf{q}_I^B)$ is the attitude matrix mapping the inertial frame to the body frame using the quaternion parameterization. Furthermore, the unit vector $\mathbf{u}_{\text{sun}}^I$ points from the SO to the Sun direction and the unit vector $\mathbf{u}_{\text{obs}}^I$ points from the SO to the observer. The vector $\mathbf{u}_h^I$ is the normalized half vector between $\mathbf{u}_{\text{sun}}^I$ and $\mathbf{u}_{\text{obs}}^I$. This vector is also known as the Sun-SO-Observer bisector. Each facet has an area $\mathcal{A}(i)$ associated with it. Once the number of facets has been defined and their basis vectors are known, the areas $\mathcal{A}(i)$ define the size and shape of the SO. To determine the SRP forces and light curve characteristics, the surface properties must be defined for each facet.

For the development of the measured light curve data, faceted SO shape models are used. An octant triangulation is used to create control points, shown in Figure 2. Control points, shown in Figure 2(a), are used to create a convex hull shape surface, shown in Figure 2(b). The control point

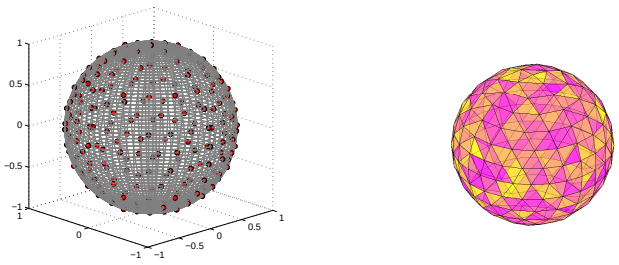

(a) Control Points on the Unit Sphere (b) Convex Shape Model

Figure 2. Space Object Shape Model

are allowed to only vary in the radial direction and therefore the shape parameters are given by $\boldsymbol{\mathcal{P}} = [p_1, ..., p_n]$ where p_i is the radial distance from the origin of the i^{th} point. Then, control points are given by the following vector:

$$\mathbf{b}_i = \mathbf{n}_i \boldsymbol{\mathcal{P}}(i) \tag{2}$$

where $\mathbf{n}_i$ the unit vector defining the direction of the control point, shown in Figure 2(a). Then the area of the i^{th} triangular facet formed by the convex hull of the control points is given by, $\mathcal{A}(i) = \|\mathbf{d}(i) \times \mathbf{l}(i)\|$, where $\mathbf{d}(i)$ and $\mathbf{l}(i)$ are the vectors defining the sides of the facets or $\mathbf{d}(i) = \mathbf{b}_i - \mathbf{b}_{i-1}$, $\mathbf{l}(i) = \mathbf{b}_i - \mathbf{b}_{i+1}$. The unit normal vector is given by

$$\mathbf{u}_n = \frac{\mathbf{d}(i) \times \mathbf{l}(i)}{\|\mathbf{d}(i) \times \mathbf{l}(i)\|} \tag{3}$$

For this work it is assumed that each facet has the same material parameters.

SYSTEM MODELS

Orbital and Attitude System Model

In this paper the position and velocity of an Earth orbiting RSO are denoted by $\mathbf{r} = [x \;\; y \;\; z]^T$ and velocity $\mathbf{v} = [v_x \;\; v_y \;\; v_z]^T$ respectively. The two-body equations of motion are given by

$$\ddot{\mathbf{r}}^I = -\frac{\mu}{r^3}\mathbf{r}^I - \mathbf{a}_{J_2} + \mathbf{a}^I_{\text{srp}} \tag{4}$$

where μ is the gravitational parameter of the Earth, $r = \|\mathbf{r}^I\|$, $\mathbf{a}_{J_2}$ is the gravitational perturbation due to non-symmetric distribution of mass along the lines of latitude of the Earth and $\mathbf{a}^I_{\text{srp}}$ represents the acceleration perturbation due to SRP, which will be discussed in detail in the following section. The acceleration due to the J_2 effect is given by

$$\mathbf{a}_{J_2} = \frac{3}{2} J_2 \left(\frac{\mu}{r^2}\right) \left(\frac{R_\oplus}{r}\right)^2 \begin{bmatrix} \left(1 - 5\left(\frac{z}{r}\right)^2\right)\frac{x}{r} \\ \left(1 - 5\left(\frac{z}{r}\right)^2\right)\frac{y}{r} \\ \left(3 - 5\left(\frac{z}{r}\right)^2\right)\frac{z}{r} \end{bmatrix} \mathbf{r}^I \tag{5}$$

where J_2 is the coefficient for the second zonal harmonic, $R_\oplus$ is the mean equatorial radius of the Earth.

A number of parameterizations exist to specify attitude, including Euler angles, quaternions, and Rodrigues parameters.[13] This paper uses the quaternion, which is based on the Euler angle/axis parametrization. The quaternion is defined as $\mathbf{q} \equiv [\boldsymbol{\varrho}^T \quad q_4]^T$ with $\boldsymbol{\varrho} = \hat{\mathbf{e}} \sin(\nu/2)$, and $q_4 = \cos(\nu/2)$, where $\hat{\mathbf{e}}$ and ν are the Euler axis of rotation and rotation angle, respectively. Clearly, the quaternion must satisfy a unit norm constraint, $\mathbf{q}^T\mathbf{q} = 1$. In terms of the quaternion, the attitude matrix is given by

$$A = \Xi^T(\mathbf{q})\Psi(\mathbf{q}) \tag{6}$$

where

$$\Xi(\mathbf{q}) \equiv \begin{bmatrix} q_4 I_{3\times 3} + [\boldsymbol{\varrho}\times] \\ -\boldsymbol{\varrho}^T \end{bmatrix} \tag{7a}$$

$$\Psi(\mathbf{q}) \equiv \begin{bmatrix} q_4 I_{3\times 3} - [\boldsymbol{\varrho}\times] \\ -\boldsymbol{\varrho}^T \end{bmatrix} \tag{7b}$$

with

$$[\mathbf{a}\times] = \begin{bmatrix} 0 & -a_3 & a_2 \\ a_3 & 0 & -a_1 \\ -a_2 & a_1 & 0 \end{bmatrix} \tag{8}$$

for any general 3×1 vector $\mathbf{a}$ defined such that $[\mathbf{a}\times]\mathbf{b} = \mathbf{a} \times \mathbf{b}$.

The rotational dynamics are given by the coupled first order differential equations

$$\dot{\boldsymbol{\omega}} = J_{\text{RSO}}^{-1}\left(T_{\text{srp}}^B - \left[\boldsymbol{\omega}_{B/I}^B\times\right] J_{\text{RSO}}\boldsymbol{\omega}_{B/I}^B\right) \tag{9a}$$

$$\dot{\mathbf{q}} = \frac{1}{2}\Xi(\mathbf{q})\boldsymbol{\omega}_{B/I}^B \tag{9b}$$

where $\boldsymbol{\omega}_{B/I}^B$ is the angular velocity of the RSO with respect to the inertial frame, expressed in body coordinates, J_{RSO} is the inertia matrix of the RSO and T_{srp}^B is the net torque acting on the RSO due to SRP expressed in body coordinates.

Solar Radiation Pressure Model

For higher altitude objects ($\geq$ 1,000 km), SRP represents the primary non-conservative perturbation acting on SOs. Because SRP depends on the SOs position and orientation, its effect couples the position and attitude dynamics. For an SO comprised of a collection of N flat facets as defined in Figure 1, the acceleration perturbation due to SRP is given by[14,15]

$$\mathbf{a}_{\text{srp}}^I = \sum_{i=1}^{N} \mathbf{a}_{\text{srp}}^I(i) \tag{10a}$$

$$\mathbf{a}_{\text{srp}}^I(i) = \frac{-S_F \mathcal{A}(i)\cos^2(\theta(i))\, G[\cos(\theta(i))]}{m_{\text{SO}}\, c\, d^2}\mathbf{u}_{\text{srp}}^I(i) \tag{10b}$$

$$\mathbf{u}_{\text{srp}}^I(i) = 2\left[\frac{R_{\text{diff}}(i)}{3} + \frac{R_{\text{abs}}(i)\epsilon(i)}{3} + R_{\text{spec}}(i)\cos(\theta(i))\right]\mathbf{u}_n^I(i) + [1 - R_{\text{spec}}(i)]\mathbf{u}_{\text{sun}}^I \tag{10c}$$

where $S_F = 1,367$ W/m^2 is referred to the solar constant and is a measure of the flux density of electromagnetic radiation incident on a sphere of radius 1 AU centered at the Sun, $c = 299,792,458$ m/s is the speed of light in a vaccuum, d is the distance between the SO and the Sun expressed in

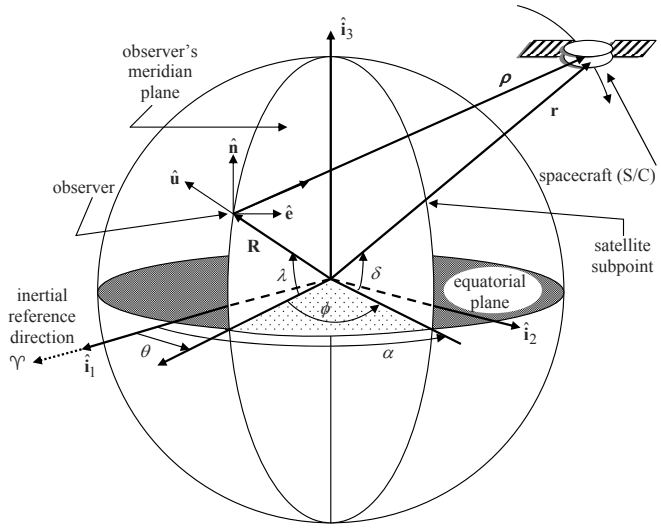

Figure 3. Geometry of Earth Observations of Spacecraft Motion

AU, m_{SO} is the mass of the SO, $\epsilon(i)$, $\mathcal{A}(i)$ and $\mathbf{u}_n^I(i)$ are the emissivity, total area and normal vector for the i^{th} facet and $R_{\text{spec}}(i)$, $R_{\text{diff}}(i)$ and $R_{\text{abs}}(i)$ are the spectral reflectance, diffuse reflectance and absorption coefficients which are assumed constant over the entire plate. Under the assumption that no energy is transmitted through the SO allows one to write

$$R_{\text{spec}}(i) + R_{\text{diff}}(i) + R_{\text{abs}}(i) = 1 \tag{11}$$

In addition, $\cos(\theta(i)) \equiv \left(\mathbf{u}_n^I(i)\right)^T \mathbf{u}_{\text{sun}}^I$ is the cosine of the inclination of the i^{th} facet towards the Sun. The function $G[a] \equiv \max[0, \text{sign}(a)]$ will be zero when a side is shaded from the Sun (i.e. $\cos(\theta(i)) \leq 0$) and one when the facet is illuminated.

Equation (10b) can also be used in determining the torque on the SO due to SRP. Because the spectral, diffuse and absorption coefficients are constant over the entire facet, the contribution of SRP over the entire facet can be assumed to be a single force acting on the centroid of the facet. The total torque is then given by

$$T_{\text{srp}}^B = m_{\text{SO}} \sum_{i=1}^{N} \left[\boldsymbol{\ell}^B(i)\times\right] \left(A(\mathbf{q}_I^B)\mathbf{a}_{\text{srp}}^I(i)\right) \tag{12}$$

where $\boldsymbol{\ell}^B(i)$ is the position vector from the center of mass of the SO to the centroid of i^{th} facet.

Observation Model

The observation system is shown in Figure 3. Consider observations made by a optical site which measures azimuth and elevation to a SO. The vector $\mathbf{d}^I$ is the position vector from the observer to the SO, $\mathbf{r}^I$ is the position of the SO in inertial coordinates, $\mathbf{R}^I$ is the radius vector locating the observer, α and δ are the right ascension and declination of the SO, respectively, θ is the sidereal time of the observer, λ is the latitude of the observer, and ϕ is the East longitude from the observer to the SO. The fundamental observation is given by

$$\mathbf{d}^I = \mathbf{r}^I - \mathbf{R}^I \tag{13}$$

In non-rotating equatorial (inertial) components the vector $\mathbf{d}^I$ is given by

$$\mathbf{d}^I = \begin{bmatrix} x - ||\mathbf{R}^I|| \cos(\theta)\cos(\lambda) \\ y - ||\mathbf{R}^I|| \sin(\theta)\cos(\lambda) \\ z - ||\mathbf{R}^I|| \sin(\lambda) \end{bmatrix} \tag{14}$$

The conversion of $\mathbf{d}^I$ from the inertial to the observer coordinate system (Up-East-North) is given by

$$\begin{aligned} \begin{bmatrix} \rho_u \\ \rho_e \\ \rho_n \end{bmatrix} = & \begin{bmatrix} \cos(\lambda) & 0 & \sin(\lambda) \\ 0 & 1 & 0 \\ -\sin(\lambda) & 0 & \cos(\lambda) \end{bmatrix} \\ & \times \begin{bmatrix} \cos(\theta) & \sin(\theta) & 0 \\ -\sin(\theta) & \cos(\theta) & 0 \\ 0 & 0 & 1 \end{bmatrix} \mathbf{d}^I \end{aligned} \tag{15}$$

The angle observations consist of the azimuth, az, and elevation, el. The observation equations are given by

$$\text{az} = \tan^{-1}\left(\frac{\rho_e}{\rho_n}\right) \tag{16a}$$

$$\text{el} = \sin^{-1}\left(\frac{\rho_u}{\|\mathbf{d}^I\|}\right) \tag{16b}$$

In addition to the azimuth and elevation, the optical site also records the magnitude of the brightness of the SO. The brightness of an object in space can be modeled using a Phong light diffusion model.[16] This model is based on the bidirectional reflectance distribution function (BRDF) which models light distribution scattered from the surface due to the incident light. The BRDF at any point on the surface is a function of two directions, the direction from which the light source originates, and the direction from which the scattered light leaves the observed surface. The model in Ref. [16] decomposes the BRDF into a specular component and a diffuse component. The two terms sum to give the total BRDF

$$\rho_{\text{total}}(i) = \rho_{\text{spec}}(i) + \rho_{\text{diff}}(i) \tag{17}$$

The diffuse component of Eq. (17), $\rho_{\text{diff}}(i)$ represents light that is scattered equally in all directions (Lambertian). The specular component of Eq. (17), $\rho_{\text{spec}}(i)$ represents light that is concentrated about some direction (mirror-like). Reference [16] develops a model for continuous arbitrary surfaces but simplifies for flat surfaces which is employed in this work. Therefore, the total observed brightness of an object becomes the sum of the contribution from each facet.

Under the flat facet assumption the specular term of the BRDF becomes[16]

$$\rho_{\text{spec}}(i) = \frac{\sqrt{(n_u+1)(n_v+1)}}{8\pi} \frac{\left(\mathbf{u}_n^I(i)\cdot\mathbf{u}_h^I\right)^{n_u(\mathbf{u}_h^I\cdot\mathbf{u}_u^I(i))^2+n_v(1-(\mathbf{u}_h^I\cdot\mathbf{u}_v^I(i))^2)}}{\mathbf{u}_n^I(i)\cdot\mathbf{u}_{\text{sun}}^I + \mathbf{u}_n^I(i)\cdot\mathbf{u}_{\text{obs}}^I - (\mathbf{u}_n^I(i)\cdot\mathbf{u}_{\text{sun}}^I)(\mathbf{u}_n^I(i)\cdot\mathbf{u}_{\text{obs}}^I)} F_{\text{reflect}}(i) \tag{18a}$$

where the Fresnel reflectance is given by

$$F_{\text{reflect}}(i) = R_{\text{spec}}(i) + \left(1 - R_{\text{spec}}(i)\right)\left(1 - \mathbf{u}_{\text{sun}}^I \cdot \mathbf{u}_h^I(i)\right)^5 \tag{19}$$

The parameters n_u and n_v of the Phong model dictate the direction (locally horizontal or vertical) distribution of the specular terms. The terms in Eq. (18) are functions of the reflection geometry which is described in Figure 1. The diffuse term of the BRDF for a single facet is

$$\rho_{\text{diff}}(i) = \left(\frac{28R_{\text{diff}}(i)}{23\pi}\right)(1 - R_{\text{spec}}(i))\left[1 - \left(1 - \frac{\mathbf{u}_n^I(i)\cdot\mathbf{u}_{\text{sun}}^I}{2}\right)^5\right]\left[1 - \left(1 - \frac{\mathbf{u}_n^I(i)\cdot\mathbf{u}_{\text{obs}}^I}{2}\right)^5\right] \tag{20}$$

The apparent magnitude of a SO is the result of sunlight reflecting off of its surfaces along the line-of-sight to an observer. First, the fraction of visible sunlight that strikes an object (and not absorbed) is computed by

$$F_{\text{sun}}(i) = C_{\text{sun,vis}}\,\rho_{\text{total}}(i)\left(\mathbf{u}_n^I(i)\cdot\mathbf{u}_{\text{sun}}^I\right) \tag{21}$$

where $C_{\text{sun,vis}} = 455\ \text{W/m}^2$ is the power per square meter impinging on a given object due to visible light striking the surface. If either the angle between the surface normal and the observer's direction or the angle between the surface normal and Sun direction is greater than $\pi/2$, then there is no light reflected toward the observer. If this is the case, then the fraction of visible light is set to $F_{\text{sun}}(i) = 0$. Next, the fraction of sunlight that strikes an object that is reflected must be computed:

$$F_{\text{obs}} = \frac{F_{\text{sun}}(i)\mathcal{A}(i)\left(\mathbf{u}_n^I(i)\cdot\mathbf{u}_{\text{obs}}^I\right)}{\|\mathbf{d}^I\|^2} \tag{22}$$

The reflected light of each facet is now used to compute the total photon flux, which is measured by an observer:

$$\tilde{F} = \left[\sum_{i=1}^{N} F_{\text{obs}}(i)\right] + v_{\text{CDD}} \tag{23}$$

where v_{CDD} is the measurement noise associated with flux measured by a CCD sensor.

CCD SENSOR NOISE MODEL

The intensities of each pixel is corrupted by measurement noise. There are three main sources of noise in the intensity measurements: signal shot noise, dark current noise, and readout noise. The signal noise, which follows a poisson Process, is proportional to the stellar signal. The variance of the signal shot noise is, $\sigma_{\text{shot}}^2 = S\Delta t$, where S is the signal of the measured pixel intensity and Δt is the integration time. The dark current noise is a result of thermally generated electrons, and its variance is given by, $\sigma_{\text{dark}}^2 = d\Delta t$, where d is the dark current rate of electrons and is a function of the temperature of the sensor. Readout noise is associated with the inexact conversion of electrons, from the signal, to the digitized sensor output. The variance of the readout noise is given by, $\sigma_{\text{readout}}^2 = R\,N$, where R is the number of electrons caused by readout per pixel and N is the number of pixels considered. If this noise is to be determined for one pixel, $N = 1$. Then the total error in the intensity measurements can be written as

$$\sigma_{\text{CCD}}^2 = \sigma_{\text{readout}}^2 + \sigma_{\text{dark}}^2 + \sigma_{\text{shot}}^2 \tag{24}$$

The signal to noise ratio (SNR) can be written as

$$\text{SNR} = \frac{S}{\sqrt{S + d\Delta t + R\,N}} \tag{25}$$

UNSCENTED KALMAN FILTER FORMULATION

The unscented Kalman filter (UKF) is chosen for state estimation because it has at least the accuracy of a second-order filter[17] without the requirement of computing Jacobians like the extended Kalman filter (EKF). The UKF structure is used for estimating rotational, translational, and parameter states based on fusing angles and light curve data along with their associated models, as discussed previously. The attitude UKF described in Ref. [18] is used in the same manner as the one shown in Refs. [11] and [19].

Applying the UKF structure for attitude estimation has some challenges. For instance, although three parameter sets are attitude minimal representations, they inherently have singularities. On the other hand, the quaternion representation, which is a four parameter set with no singularity, has a nonlinear constraint which results in a singular covariance matrix, and the quaternion is not constituted by directly adding quaternions but through quaternion composition. This does not allow use of quaternions in a straightforward UKF implementation. This work uses the method in Ref. [18], which overcomes these challenges by utilizing generalized Rodrigues parameters (GRPs), a three parameter set, to define the local error and quaternions to define the global attitude. The representation of the attitude error as a GRP is useful for the propagation and update stages of the attitude covariance because the structure of the UKF can be used directly. Complete explanations of the quaternion and its mapping to GRPs are provided in Refs. [20] and [21].

In the UKF implementation described in Ref. [18], the covariance matrix is interpreted as the covariance of the error GRP because for small angle errors, the error GRP is additive and the UKF structure can be used directly to compute sigma-points. The error GRP sigma points are converted to error quaternions and then to global quaternions for the propagation stage. To compute the propagated covariance, the global quaternions are converted to error quaternions and then back to error GRPs. The process is then as follows: error GRP $\rightarrow$ error quaternion, error quaternion $\rightarrow$ global quaternion, global quaternion $\rightarrow$ error quaternion, and finally error quaternion $\rightarrow$ error GRP.

Model and Measurement Uncertainty

A UKF is now summarized for estimating the state of a SO's position, velocity, orientation, rotation rate, and control displacement given by

$$\mathbf{x} = [\mathbf{q}_I^{B^T} \;\; \boldsymbol{\omega}_{B/I}^{B^T} \;\; \mathbf{r}^{I^T} \;\; \mathbf{v}^{I^T} \;\; \boldsymbol{\mathcal{P}}^T]^T$$

The dynamic models from Eqs. (4) and (9) can be written in the general state equation which gives the deterministic part of the stochastic model:

$$\dot{\mathbf{x}} = \mathbf{f}\left(\mathbf{x}, t\right) + G\left(\mathbf{x}, t\right)\boldsymbol{\Gamma}(t), \tag{26}$$

where $\boldsymbol{\Gamma}(t)$ is a Gaussian white noise process term with correlation function $Q\delta(t_1 - t_2)$. The function $\mathbf{f}\left(\mathbf{x}, t\right)$ is a general nonlinear function. To solve the general nonlinear filtering problem, the UKF utilizes the unscented transformation to determine the mean and covariance propagation though the function $\mathbf{f}\left(\mathbf{x}, t\right)$. The dynamic function used in this work consists of rotational and translational dynamics given by the sigma points, which are propagated through the system dynamics:

$$\mathbf{f}\left([\boldsymbol{\chi}, \hat{\mathbf{q}}]\right) = \begin{bmatrix} \frac{1}{2}\Xi(\hat{\mathbf{q}})\hat{\boldsymbol{\omega}}_{B/I}^{B} \\ J_{\text{SO}}^{-1}\left(\hat{\mathbf{T}}_{\text{srp}}^{B} - \left[\hat{\boldsymbol{\omega}}_{B/I}^{B}\times\right] J_{\text{SO}}\hat{\boldsymbol{\omega}}_{B/I}^{B}\right) \\ \dot{\hat{\mathbf{r}}}^{I} \\ -\frac{\mu}{r^3}\hat{\mathbf{r}}^{I} - \hat{\mathbf{a}}_{J_2} + \hat{\mathbf{a}}_{\text{SRP}}^{I} \end{bmatrix} \tag{27}$$

If the initial pdf, $p(\mathbf{x}_o)$, that describes the associated state uncertainty is given, the solution for the time evolution of $p(\mathbf{x}, t)$ constitutes the nonlinear filtering problem.

Given a system model with initial state and covariance values, the UKF propagates the state vector and the error-covariance matrix recursively. At discrete observation times, the UKF updates the state and covariance matrix conditioned on the information gained from the measurements. The prediction phase is important for overall filter performance. In general, the discrete measurement equation can be expressed for the filter as

$$\tilde{\mathbf{y}}_k = \mathbf{h}\left(\mathbf{x}_k, t_k\right) + \mathbf{v}_k \tag{28}$$

where $\tilde{\mathbf{y}}_k$ is a measurement vector and $\mathbf{v}_k$ is the measurement noise, which is assumed to be a zero-mean Gaussian process with covariance R_k.

All random variables in the UKF are assumed to be Gaussian random variables and their distributions are approximated by deterministically selected sigma points. The sigma points are selected to be along the principal axis directions of the state error-covariance. Given an $L \times L$ error-covariance matrix P_k, the sigma points are constructed by

$$\boldsymbol{\sigma}_k \leftarrow 2L \text{ columns from } \pm\sqrt{(L+\lambda)P_k} \tag{29a}$$

$$\boldsymbol{\chi}_k(0) = \boldsymbol{\mu}_k \tag{29b}$$

$$\boldsymbol{\chi}_k(i) = \boldsymbol{\sigma}_k(i) + \boldsymbol{\mu}_k \tag{29c}$$

where $\sqrt{M}$ is shorthand notation for a matrix Z such that $M = Z\,Z^T$. Given that these points are selected to represent the distribution of the state vector, each sigma point is given a weight that preserves the information contained in the initial distribution:

$$W_0^{\text{mean}} = \frac{\lambda}{L+\lambda} \tag{30a}$$

$$W_0^{\text{cov}} = \frac{\lambda}{L+\lambda} + (1 - \alpha^2 + \beta) \tag{30b}$$

$$W_i^{\text{mean}} = W_i^{\text{cov}} = \frac{1}{2(L+\lambda)}, \quad i = 1,\, 2,\, \ldots,\, 2L \tag{30c}$$

where $\lambda = \alpha^2(L+\kappa) - L$ is a composite scaling parameter. The constant α controls the spread of the sigma point distribution and should be a small number, $0 < \alpha \leq 1$. The constant $\kappa = 3 - L$ provides an extra degree of freedom that is used to fine-tune the higher-order moments, and β is used to incorporate prior knowledge of the distribution by weighting the mean sigma point in the covariance calculation.

The reduced state vector, with the error GRP states and the full state vector, with quaternion state vector, for the joint attitude and position estimate problem are given by

$$\hat{\mathbf{x}}_k^{\boldsymbol{\delta}\mathbf{p}} = \left.\begin{bmatrix} \boldsymbol{\delta}\hat{\mathbf{p}}_I^B \\ \boldsymbol{\delta}\hat{\mathbf{p}}_P^B \\ \hat{\boldsymbol{\omega}}_{B/I}^B \\ \hat{\mathbf{r}}^I \\ \hat{\mathbf{v}}^I \\ \boldsymbol{\mathcal{P}} \end{bmatrix}\right|_{t_k} \tag{31}$$

where $\boldsymbol{\delta}\hat{\mathbf{p}}$ are the error GRP states associated with the quaternion $\hat{\mathbf{q}}_I^B$ and $\hat{\cdot}$ is used to denote estimate. The initial estimate $\hat{\mathbf{x}}_0$ is the mean sigma point and is denoted $\boldsymbol{\chi}_0(0)$. The error GRP state of the initial estimate is set to zero, while the rest of the states are initialized by their respective initial estimates.

Quaternion-Based UKF

The error quaternion, denoted by $\boldsymbol{\delta}\mathbf{q}_k^-(i)$, associated with the i^{th} error GRP sigma point is computed by[18]

$$\boldsymbol{\delta\varrho}_k^-(i) = f^{-1}\left[a + \delta q_{4_k}^-(i)\right]\boldsymbol{\chi}_k^{\delta p}(i) \tag{32a}$$

$$\delta q_{4_k}^-(i) = \frac{-a||\boldsymbol{\chi}_k^{\delta p}(i)||^2 + f\sqrt{f^2 + (1-a^2)||\boldsymbol{\chi}_k^{\delta p}(i)||^2}}{f^2 + ||\boldsymbol{\chi}_k^{\delta p}(i)||^2} \tag{32b}$$

$$\boldsymbol{\delta}\mathbf{q}_k^-(i) = \begin{bmatrix}\boldsymbol{\delta\varrho}_k^-(i)\\ \delta q_{4_k}^-(i)\end{bmatrix} \tag{32c}$$

where a is a parameter from 0 to 1 and f is a scale factor, which is often set to $f = 2(a+1)$. The representation of the attitude estimate perturbed by the i^{th} error quaternion is computed using the quaternion composition:

$$\hat{\mathbf{q}}_k^-(i) = \boldsymbol{\delta}\mathbf{q}_k^-(i) \otimes \hat{\mathbf{q}}_k^-(0) \tag{33}$$

where

$$\mathbf{q}' \otimes \mathbf{q} = \begin{bmatrix}\Psi(\mathbf{q}') & \mathbf{q}'\end{bmatrix}\mathbf{q} \tag{34}$$

This forms the global quaternion. The error quaternions corresponding to each propagated quaternion sigma point are computed through the quaternion composition:

$$\boldsymbol{\delta}\mathbf{q}_{k+1}^-(i) = \hat{\mathbf{q}}_{k+1}^-(i) \otimes \left[\hat{\mathbf{q}}_{k+1}^-(0)\right]^{-1} \tag{35}$$

where the notation for the inverse quaternion is defined as:

$$\mathbf{q}^{-1} \equiv \begin{bmatrix} -\boldsymbol{\varrho} \\ q_4 \end{bmatrix} \tag{36}$$

Using the result of Eq. (35), the error GRP sigma points are computed as

$$\boldsymbol{\delta}\mathbf{p}_{k+1}^-(i) = f\frac{\boldsymbol{\delta}\hat{\boldsymbol{\varrho}}_{k+1}^-(i)}{a + \delta\hat{q}_{4_{k+1}}^-(i)} \tag{37}$$

Angles data can be used to determine the unknown position and velocity of a SO. However, if the position is coupled with the attitude dynamics, then angles data can assist with attitude estimation as well. However if position is known accurately, then using only light curve data is sufficient to determine the orientation.

Table 1. UKF for Rotational, Translational, and Parameter States

Initialize with $\hat{\mathbf{x}}_o^{\boldsymbol{\delta}\mathbf{p}} = E\{\mathbf{x}_o^{\boldsymbol{\delta}\mathbf{p}}\} \quad \hat{\mathbf{x}}_o^{\mathbf{q}} = E\{\mathbf{x}_o\} \quad \mathbf{P}_o^{\boldsymbol{\delta}\mathbf{p}} = E\{\left(\mathbf{x}_o^{\boldsymbol{\delta}\mathbf{p}} - \hat{\mathbf{x}}_o^{\boldsymbol{\delta}\mathbf{p}}\right)\left(\mathbf{x}_o^{\boldsymbol{\delta}\mathbf{p}} - \hat{\mathbf{x}}_o^{\boldsymbol{\delta}\mathbf{p}}\right)^T\}$
Calculate GRP Sigma Points $\boldsymbol{\chi}_k^{\boldsymbol{\delta}\mathbf{p}} = \left[\hat{\mathbf{x}}_k^{\boldsymbol{\delta}\mathbf{p}} \quad \hat{\mathbf{x}}_k^{\boldsymbol{\delta}\mathbf{p}} + \gamma\sqrt{P_{k-1}} \quad \hat{\mathbf{x}}_k^{\boldsymbol{\delta}\mathbf{p}} - \gamma\sqrt{P_{k-1}}\right]$ Calculate Quaternion Sigma Points $\boldsymbol{\chi}_k^{\mathbf{q}} = \left[\hat{\mathbf{x}}_k^{\mathbf{q}} \quad \hat{\mathbf{x}}_k^{\mathbf{q}} + \gamma\sqrt{P_{k-1}} \quad \hat{\mathbf{x}}_k^{\mathbf{q}} - \gamma\sqrt{P_{k-1}}\right]$
Propagate Quaternion Sigma Points $\boldsymbol{\chi}_k^{\mathbf{q}} = \mathbf{F}\left[\boldsymbol{\chi}_{k-1}^{\mathbf{q}}, t\right]$ Calculate GRP Sigma Points $\boldsymbol{\chi}_k^{\boldsymbol{\delta}\mathbf{p}} = \left[\hat{\mathbf{x}}_k^{\boldsymbol{\delta}\mathbf{p}} \quad \hat{\mathbf{x}}_k^{\boldsymbol{\delta}\mathbf{p}} + \gamma\sqrt{P_{k-1}} \quad \hat{\mathbf{x}}_k^{\boldsymbol{\delta}\mathbf{p}} - \gamma\sqrt{P_{k-1}}\right]$
Time update $\hat{\mathbf{x}}_{k+1}^- = \sum_{i=0}^{2L} W_i^{\text{mean}} \boldsymbol{\chi}_{k+1}(i)$ $P_{k+1}^- = \sum_{i=0}^{2L} W_i^{\text{cov}} \left[\boldsymbol{\chi}_{k+1}(i) - \hat{\mathbf{x}}_{k+1}^-\right]\left[\boldsymbol{\chi}_{k+1}(i) - \hat{\mathbf{x}}_{k+1}^-\right]^T + Q_{k+1}$
Measurement update $\boldsymbol{\gamma}_k(i) = \mathbf{h}\left[\boldsymbol{\chi}_k(i), \hat{\mathbf{q}}_k^-\right]$ $\hat{\mathbf{y}}_k^- = \sum_{i=0}^{2L} W_i^{\text{mean}} \boldsymbol{\gamma}_k(i)$ $P_k^{yy} = \sum_{i=0}^{2L} W_i^{\text{cov}} \left[\boldsymbol{\gamma}_k(i) - \hat{\mathbf{y}}_k^-\right]\left[\boldsymbol{\gamma}_k(i) - \hat{\mathbf{y}}_k^-\right]^T$ $P_k^{vv} = P_k^{yy} + R_k$ $P_k^{xy} = \sum_{i=0}^{2L} W_i^{\text{cov}} \left[\boldsymbol{\chi}_k(i) - \hat{\mathbf{x}}_k^-\right]\left[\boldsymbol{\gamma}_k(i) - \hat{\mathbf{y}}_k^-\right]^T$ $K_k = P_k^{xy}(P_k^{vv})^{-1}$ $\hat{\mathbf{x}}_k^+ = \hat{\mathbf{x}}_k^- + K_k\left[\tilde{\mathbf{y}}_k - \hat{\mathbf{y}}_k\right]$ $P_k^+ = P_k^- - K_k P^{vv} K_k^T$
Quaternion update $\hat{\mathbf{q}}_k^+ = \boldsymbol{\delta}\hat{\mathbf{q}}_k^+ \otimes \hat{\mathbf{q}}_k^-(0)$ Set GRP to zero $\boldsymbol{\delta}\mathbf{p} = [0 \quad 0 \quad 0]^T$

Summary of UKF

The UKF algorithm is described in Table 1. The process starts by first defining two initial state vectors, one that includes quaternion states and one that includes error GRP states. The error GRP states are initially set to zero. The initial covariance matrix is defined as the initial error covariance for the state vector that includes the GRP states, the translational, rotational and parametric states. The covariance matrix is then used to form the error GRP sigma points. The error GRP sigma points are converted to quaternion sigma points by creating error quaternions from each error GRP and then adding the error quaternion to the initial mean quaternion using quaternion multiplication.

Next the quaternion sigma points are propagated through the system dynamics in Eq. (27). The estimated acceleration and torque due to SRP are calculated with Eqs. (10) and (12), respectively. After propagating the sigma points, the error GRP states are computed with the propagated quaternion sigma points. The propagated mean sigma point quaternion, $\hat{\mathbf{q}}^{-}_{k+1}(0)$, is computed and stored, and error quaternions corresponding to each propagated quaternion sigma point are computed. The non-attitude sigma points are the propagated non-attitude states.

After setting the error GRP for the mean sigma point to zero, the propagated sigma points are recombined, and the propagated mean and covariance are calculated as a weighted sum of the sigma points, where Q_{k+1} is the discrete-time process noise covariance. As previously discussed, measurements are available in the form of azimuth, elevation and apparent brightness magnitude, $\tilde{\mathbf{y}} \equiv [\tilde{m}_{\text{app}} \quad \tilde{\text{az}} \quad \tilde{\text{el}}]^T$. Estimated observations are computed for each sigma point using the observation models discussed previously. The mean estimated output are computed, and the output, innovations, and cross-correlation covariance are computed using the sigma points.

Finally, the Kalman gain is calculated from the sigma point and is used to update the estimated state vector that contains the error GRPs. The quaternion update is performed by converting the error GRP states of $\hat{\mathbf{x}}^{+}_{k}$ to a quaternion, $\boldsymbol{\delta}\hat{\mathbf{q}}^{+}_{k}$, via Eq. (32), and adding it to the estimated quaternion using quaternion multiplication.

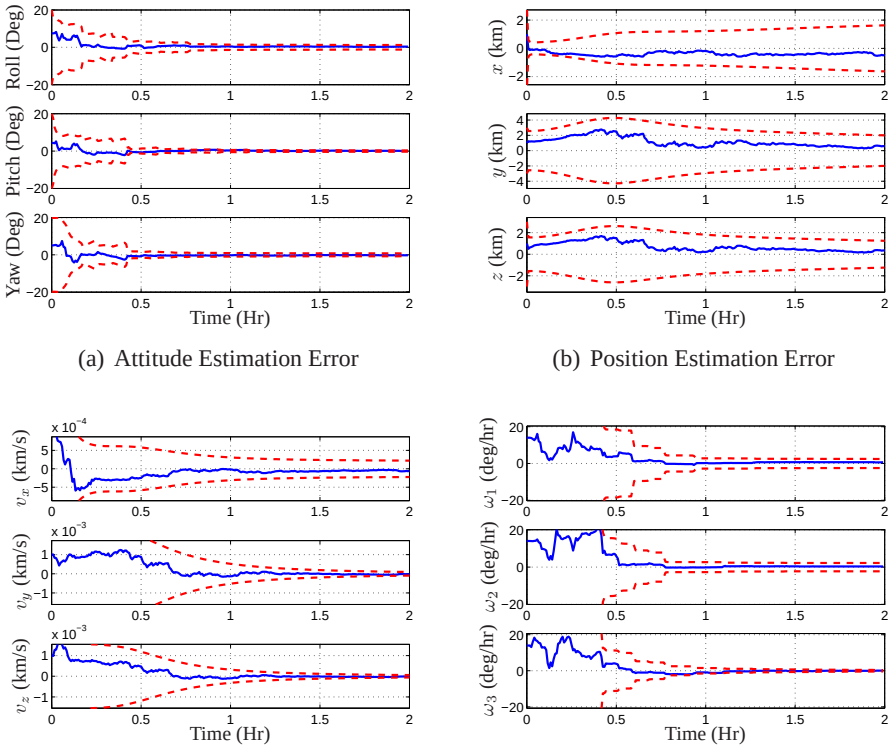

(a) Attitude Estimation Error

(b) Position Estimation Error

(c) Velocity Estimation Error

(d) Angular Velocity Estimation Error

Figure 4. SO State Estimation Results

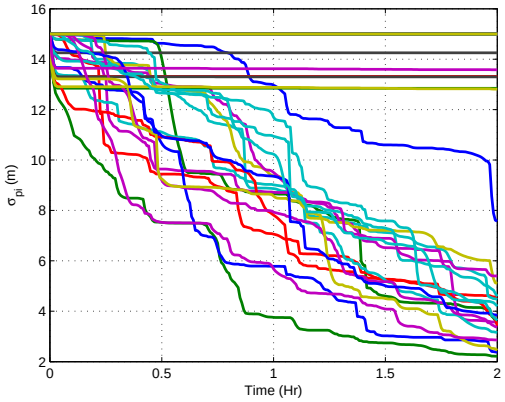

Figure 5. Standard Deviation of Shape Parameters

SIMULATION RESULTS

A simulation is presented to determine the estimator's performance. An equatorial ground station is chosen as the site of the observer for the truth model. In addition, the scenario uses a shape model which contains six sides. The SO is simulated to orbit in a continuously sunlit near-geosynchronous regime. This is accomplished by inclining the orbit by 30 degrees and choosing an appropriate time of the year, thereby avoiding the shadow cast by the Earth.

The initial inertial position and velocity are chosen as $\mathbf{r}^I = [-1.4365\times10^4 \;\; 3.8969\times10^4 \;\; 7.2715\times 10^3]^T$ km and $\mathbf{v}^I = [-2.8906 \;\; -1.0318 \;\; -0.1811 \times 10^{-1}]^T$ km/s. The geographic position of the ground site is 0° North, 172° West with 0 km altitude. The time epoch of the simulation is May 8, 2007 at 5:27.55. The initial true quaternion attitude mapping from the inertial frame to the body frame is chosen as $\mathbf{q}_I^B = [0 \;\; 0.1256 \;\; -0.4101 \;\; 0.9033]^T$. A constant rotation rate, defined as the body rate with respect to the inertial frame, represented in body coordinates, is used and given by $\boldsymbol{\omega}_{B/I}^B = [0 \;\; 0.00262 \;\; 0]^T$ rad/s.

For the simulation scenario, measurements are generated using zero-mean white-noise error processes with standard deviation of 0.5 arc-seconds for azimuth and elevation. The initial errors for the states are 1 km and 0.001 km/s for the position and the velocity, respectively. The initial condition error-covariance values are set to 1^2 km^2 and 0.001^2 (km/s)^2 for the position and the velocity errors, respectively. The time interval between the measurements is set to 20 seconds. Data are simulated for 1 night where observations of the SO are made over a 2 hour period.

The estimation errors, along with their respective 3σ bounds calculated from the covariance for attitude, position, velocity, rotation rate, are shown in Figure 4. The attitude is estimated to within 10° 3σ of uncertainty, and attitude rate is found to within 20 deg/hr 3σ for the x-axis, y-axis, and z-axis. Position and velocity are estimated to within 10 m and 0.0028 m/s, respectively.

The control point displacements are estimated to within 5 percent 3σ. Figure 6(b) shows the estimated shape and figure 6(a) shows three shape parameter estimates with their respective 3σ bounds. Figure 5 shows the standard deviations for each of the 48 parameters and shows that some of the parameters are not completely observable. This is due to the fact that the spin of SO does not allow the observer to see this part of the SO's geometry. Although these parameters are weakly observable, the filter can still observe the remaining control point displacements.

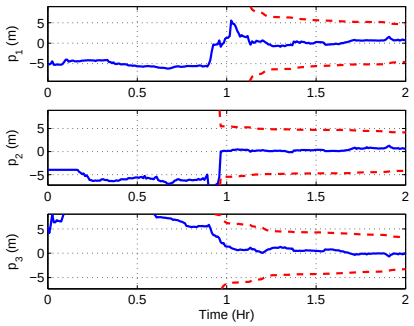

(a) Shape Parameter Errors

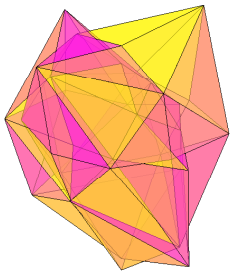

(b) Estimated SO Shape

CONCLUSION

An UKF estimation scheme using light curve and angles data was used to estimate the control points of an octant triangulation shape model, where the points are used to form a convex hull shape model made of triangular facets. The SO's associated rotational and translational states are included in the estimation process. Using a UKF to employ photon flux and angles data, the estimator was able to determine the control point displacements of an SO to within 5 percent. Simulations were conducted to study estimate accuracy. Adequate performance was found for the estimator and the errors were within the 3σ bounds.

REFERENCES

[1] Sato, T., Wakayama, T., Tanaka, T., Ikeda, K.-i., and Kimura, I., "Shape of Space Debris as Estimated from Radar Cross Section Variations," *Journal of Spacecraft and Rockets*, Vol. 31, No. 4, Oct. 1994, pp. 665–670.

[2] Walker, J. L., "Range-Doppler Imaging of Rotating Objects," *IEEE Transactions on Aerospace and Electronics Systems*, Vol. AES-16, No. 4, Jan. 1980, pp. 23–52.

[3] Hagfors, T., "Mapping Planetary Surfaces by Radar," *Proceedings of the IEEE*, Vol. 61, No. 9, Jan. 1973, pp. 1219.

[4] DiMatteo, J., Florakis, D., Weichbrod, A., and Milam, M., "Proximity Operations Testing with a Rotating and Translating Resident Space Object," *AIAA Guidance, Navigation and Control Conference*, Aug. 2009, AIAA-2009-6293.

[5] Lichter, M. D. and Dubowsky, S., "State, Shape, and Parameter Estimation of Space Objects from Range Images," *Proceedings of Robotics: Science and Systems*, June 2005.

[6] Young, G.-S. J. and Chellappa, R., "3-D Motion Estimation using a Sequence of Noisy Stereo Images: Models, Estimation, and Uniqueness Results," *IEEE Transactions on Pattern Analysis and Machine Intelligance*, Vol. 12, No. 8, 1990, pp. 735–759.

[7] Broida, T. J. and Chellappa, R., "Estimating the Kinematics and Structure of a Rigid Object from a Sequence of Monocular Images," *IEEE Transactions on Pattern Analysis and Machine Intelligence*, Vol. 13, No. 6, 1991, pp. 497–513.

[8] Kaasalainen, M. and Torppa, J., "Optimization Methods for Asteriod Lightcurve Inversion I: Shape Determination," *Icarus*, Vol. 153, No. 4, Jan. 2001, pp. 24–36.

[9] Kaasalainen, M. and Torppa, J., "Optimization Methods for Asteriod Lightcurve Inversion II: The Complete Inverse Problem," *Icarus*, Vol. 153, No. 4, Jan. 2001, pp. 37–51.

[10] Calef, B., Africano, J., Birge, B., Hall, D., and Kervin, P., "Photometric Signature Inversion," *Proceedings of the International Society for Optical Engineering*, Vol. 6307, Aug. 2006, Paper 11.

[11] Jah, M. and Madler, R., "Satellite Characterization: Angles and Light Curve Data Fusion for Spacecraft State and Parameter Estimation," *Proceedings of the Advanced Maui Optical and Space Surveillance Technologies Conference*, Vol. 49, Wailea, Maui, HI, Sept. 2007, Paper E49.

[12] Centinello, F. J., "Six Degree of Freedom Estimation with Light Curve Data," Tech. rep., AFRL, Kihei, HI, 2008.

[13] Shuster, M. D., "A Survey of Attitude Representations," *Journal of the Astronautical Sciences*, Vol. 41, No. 4, Oct.-Dec. 1993, pp. 439–517.

[14] Borderies, N. and Longaretti, P., "A New Treatment of the Albedo Radiation Pressure in the Case of a Uniform Albedo and of a Spherical Satellite," *Celestial Mechanics and Dynamical Astronomy*, Vol. 49, No. 1, March 1990, pp. 69–98.

[15] Vallado, D. A., *Fundamentals of Astrodynamics and Applications*, McGraw-Hill, New York, NY, 3^{rd} ed., 1997.

[16] Ashikmin, M. and Shirley, P., "An Anisotropic Phong Light Reflection Model," Tech. Rep. UUCS-00-014, University of Utah, Salt Lake City, UT, 2000.

[17] Julier, S. J., Uhlmann, J. K., and Durrant-Whyte, H. F., "A New Method for the Nonlinear Transformation of Means and Covariances in Filters and Estimators," *IEEE Transactions on Automatic Control*, Vol. AC-45, No. 3, March 2000, pp. 477–482.

[18] Crassidis, J. L. and Markley, F. L., "Unscented Filtering for Spacecraft Attitude Estimation," *Journal of Guidance, Control and Dynamics*, Vol. 26, No. 4, July-Aug. 2003, pp. 536–542.

[19] Wetterer, C. J. and Jah, M., "Attitude Estimation from Light Curves," *Journal of Guidance, Control and Dynamics*, Vol. 32, No. 5, Sept.-Oct. 2009, pp. 16482.

[20] Shuster, M. D., "A Survey of Attitude Representations," *Journal of the Astronautical Sciences*, Vol. 41, No. 4, Oct.-Dec. 1993, pp. 439–517.

[21] Schaub, H. and Junkins, J. L., "Stereographic Orientation Parameters for Attitude Dynamics: A Generalization of the Rodrigues Parameters," *Journal of the Astronautical Sciences*, Vol. 44, No. 1, Jan.-March 1996, pp. 1–20.